In situ study of the endotaxial growth of hexagonal CoSi2 nanoplatelets in Si(001)

Daniel da Silva Costa, Cristián Huck-Iriart, Guinther Kellermann, Lisandro J. Giovanetti, Aldo F. Craievich, and Félix G. Requejo

Citation: Applied Physics Letters **107**, 223101 (2015); doi: 10.1063/1.4936377
View online: http://dx.doi.org/10.1063/1.4936377
View Table of Contents: http://scitation.aip.org/content/aip/journal/apl/107/22?ver=pdfcov
Published by the AIP Publishing

In situ study of the endotaxial growth of hexagonal $CoSi_2$ nanoplatelets in Si(001)

Daniel da Silva Costa,[1] Cristián Huck-Iriart,[2] Guinther Kellermann,[1,a)]
Lisandro J. Giovanetti,[2] Aldo F. Craievich,[3] and Félix G. Requejo[2]
[1]*Departamento de Física, Universidade Federal do Paraná, Caixa Postal 19044, Curitiba, Paraná 81531-990, Brazil*
[2]*Instituto de Investigaciones Fisicoquímicas Teóricas y Aplicadas (INIFTA, CONICET, Departamento de Química, Facultad de Ciencias Exactas, Universidad Nacional de La Plata), CC/16 suc. 4, 1900 La Plata, Argentina*
[3]*Instituto de Física, Universidade de São Paulo, CP 66318, CEP 05315-970, São Paulo, Brazil*

(Received 21 August 2015; accepted 10 November 2015; published online 30 November 2015)

This investigation aims at studying–by *in situ* grazing-incidence small-angle x-ray scattering–the process of growth of hexagonal $CoSi_2$ nanoplatelets endotaxially buried in a Si(001) wafer. The early formation of spherical Co nanoparticles with bimodal size distribution in the deposited silica thin film during a pretreatment at 500 °C and their subsequent growth at 700 °C were also characterized. Isothermal annealing at 700 °C promotes a drastic reduction in the number of the smallest Co nanoparticles and a continuous decrease in their volume fraction in the silica thin film. At the same time, Co atoms diffuse across the SiO_2/Si(001) interface into the silicon wafer, react with Si, and build up thin hexagonal $CoSi_2$ nanoplatelets, all of them with their main surfaces parallel to Si{111} crystallographic planes. The observed progressive growths in thickness and lateral size of the hexagonal $CoSi_2$ nanoplatelets occur at the expense of the dissolution of the small Co nanoparticles that are formed during the pretreatment at 500 °C and become unstable at the annealing temperature (700 °C). The kinetics of growth of the volume fraction of hexagonal platelets is well described by the classical Avrami equation.
[http://dx.doi.org/10.1063/1.4936377]

During the last decades, a number of authors have investigated the formation of nano-objects deposited to or grown on external surfaces of different single crystalline substrates.[1–10] The knowledge of the relevant features and the control of the growth processes of these nanostructures are of particular relevance because the properties of these materials strongly depend on the sizes and shapes of the basic building blocks.[11–17] In the particular case of silicides obtained by deposition of transition metals on silicon single-crystals under ultra-high vacuum conditions, they self-assemble into high aspect ratio nanowires.[18,19] These nanostructures grow epitaxially on the silicon surface or may evolve into the silicon via endotaxial growth processes.

Endotaxial growth of nanostructures has been reported for Fe, Co, Ni, and Ti on Si(001) and Si(011).[20] In particular, $CoSi_2$ exhibits a relatively low electrical resistivity (10–15 $\mu\Omega$ cm), similar to the resistivity of $TiSi_2$ currently being used as a ohmic contact in electronic devices, and remains stable up to rather high temperatures.[21] These interesting properties allied to possibility of controlling the size of $CoSi_2$ platelets in nanoscale level make this nanostructured material a good candidate as conductive component for integrated Si circuits to be used in high speed electronic devices for applications in nanoelectronics.[3,16,22,23]

Concerning the structural characterization, the grazing-incidence small-angle x-ray scattering (GISAXS) technique had been proved to be a very reliable and useful technique to for characterizing of nanoparticles embedded or deposited on thin films.[24–26] GISAXS technique has been also successfully applied to follow the kinetic of growth of a number of nanostructures on thin films prepared under several different deposition conditions and thermal treatments.[27–30]

Co-doped SiO_2 thin films deposited on top of a Si (001) single crystalline wafer and submitted to isothermal treatment at 750 °C were recently investigated by combining *ex-situ* GISAXS and transmission electron microscopy (TEM).[9] This study evidenced the formation of spherical Co nanoparticles embedded in the supported SiO_2 thin film and also hexagonal $CoSi_2$ nanoplatelets endotaxially grown in the Si single crystal substrate.[9] Interestingly, all buried $CoSi_2$ nanoplatelets are parallel to crystallographic Si{111} planes and have their lattice coherently related to the face centered cubic lattice of the Si host, regardless the silicon face in contact with the SiO_2 film (001, 011, or 111).[10] The formation of $CoSi_2$ nanoplatelets is the result of a complex combination of physicochemical processes—such as diffusion of atoms in solid phases and chemical reaction of Co with Si—leading to the final silicide.[19,31]

The final size, shape, and ordering of the $CoSi_2$ platelets buried in Si(001) obtained after long periods of thermal treatments (1 h at 750 °C) were determined in previous *ex situ* GISAXS and TEM studies.[9,10] However, the mechanisms involved in the processes of nucleation and growth of these nanoparticles are so far not known. In order to obtain new information related to the kinetics of the process and the mechanisms involved in the early stages of crystals nucleation and growth, the endotaxial growth of $CoSi_2$ nanoplatelets is here

[a)]Author to whom correspondence should be addressed. Electronic mail: keller@fisica.ufpr.br.

studied by *in situ* GISAXS, during isothermal treatment at 700 °C of a Co-doped SiO_2 thin deposited on Si(100) wafer. *In situ* structural characterization of the nucleation and growth processes is necessary for further tailoring of nanocomponents with desired size-dependent properties.

Our *in situ* GISAXS measurements were conducted by placing the sample inside a high temperature chamber operating under He flux of 50 sccm at 700 °C. The GISAXS patterns corresponding to 8, 48, and 168 min of thermal treatment at 700 °C are shown in the left column of Fig. 1. The GISAXS patterns corresponding to increasing periods of time at 700 °C were analyzed by applying the model described in Ref. 9 that assumes the total intensity as composed of independent contributions from dilute sets of spherical Co nanoparticles embedded in silica film and hexagonal $CoSi_2$ platelets endotaxially grown in the Si(001) wafer.

The modelled 2D GISAXS patterns displayed in the right column of Figure 1 are the best fit of the function given in Ref. 9 to the experimental patterns shown in the left column. For additional description of the GISAXS procedure, analysis, and modeling, see the supplementary material.[32]

Figure 2 displays the time dependence of the volume weighted radius distribution of the spherical Co nanoparticles—determined as $V_{sph}(R) = (4\pi/3)R^3 N_{\mathrm{sph}}(R)$—embedded in the SiO_2 thin film. The results clearly indicate that the volume weighted radius distribution of Co nanoparticles is a two-mode function, i.e., there are two nanoparticle populations with different average radii, namely, $\langle R \rangle \sim 1.0$ nm (mode I) and $\langle R \rangle \sim 3.5$ nm (mode II).

The total number of smaller (mode I) Co nanoparticles decreases for increasing periods of time, approximately preserving both the average radius and size dispersion. On the other hand, the time variation corresponding to larger (mode II) Co nanoparticles indicates only a progressive widening of their radius distribution.

Time dependence of the volume weighted radius distribution of spherical Co particles displayed in Figure 2 also

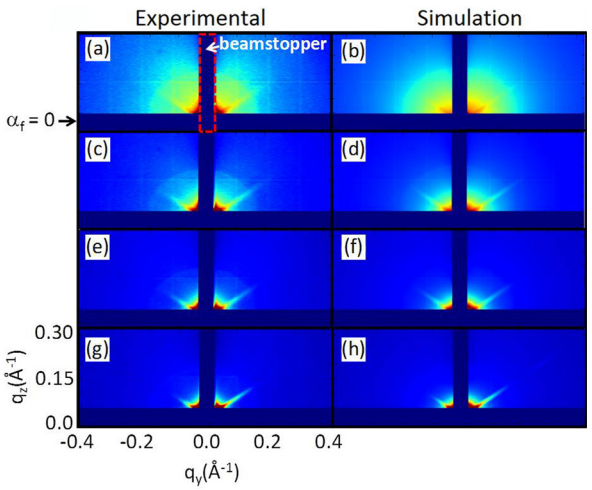

FIG. 1. 2D GISAXS patterns corresponding to the sample held at 700 °C during different periods of time: (a) and (b) 8, (c) and (d) 22, (e) and (f) 48, and (g) and (h) 168 min. The left column displays the experimental GISAXS patterns, and the right column shows the related calculated GISAXS patterns that yielded the best fit to the experimental results. The vertical stripe in the center of all patters is the shadow of the beam-stopper, and $\alpha_f = 0$—only shown for (a)—indicates the sample horizon.

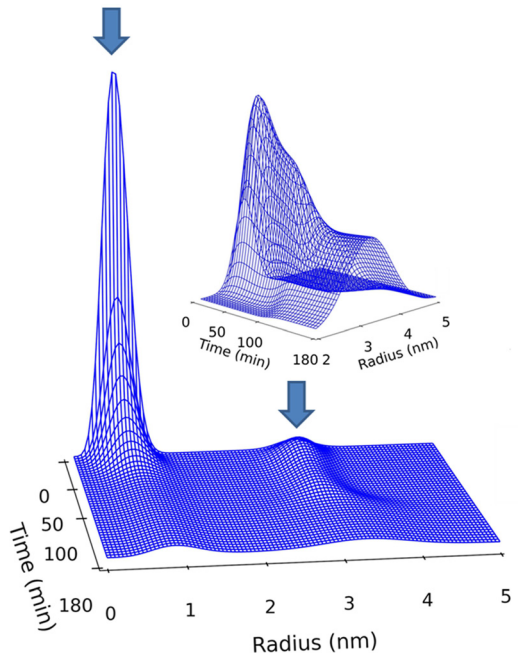

FIG. 2. Time dependence of the bimodal volume weighted radius distribution of spherical Co nanoparticles embedded in the SiO_2 thin film. Size modes I and II are indicated by arrows. The inset shows mode II in different scale and perspective.

indicates that these nanoparticles are already formed at the very beginning of the isothermal treatment at 700 °C. This implies that the nucleation of metallic Co nanoparticles had occurred during the pretreatment at 500 °C for reduction of Co precursor, i.e., before starting the final isothermal annealing at 700 °C. Result plotted in Figure 2 indicates that the total volume of Co particles with smaller radii—corresponding to the integral of the peak of mode I—strongly decreases for increasing periods of time.

Time dependences of relevant size parameter of the hexagonal $CoSi_2$ nanoplatelets, i.e., lateral side L and thickness T, and their number density N_{hex}, are plotted in Figures 3(a)–(c), respectively. The results displayed in Figures 3(a) and 3(b) show the parallel growth in thickness and lateral size, respectively, of the $CoSi_2$ nanoplatelets until both parameters reach final constant values after approximately 80 min of isothermal annealing. The results displayed in Figure 3(a) indicate that the lateral size of the hexagonal nanoplatelets, L, exhibits a fast growth from zero up to 22 nm within a few minutes of isothermal treatment at 700 °C and still growing until reaching a value $L = 30$ nm after 80 min. A similar trend is apparent for the thickness of the $CoSi_2$ nanoplatelets (Figure 3(b)), which reaches a value $T = 1.8$ nm within a few minutes and then increases up to a final constant value $T = 2.6$ nm after 80 min of isothermal treatment.

The simultaneous growth of the lateral size and thickness of $CoSi_2$ nanoplatelets shown in Figures 3(a) and 3(b), respectively, indicate that the diffusion of Co atoms along the Si{111} planes is initially very fast, thus leading to a quick formation of a few atoms thick $CoSi_2$ buried layers. Later on, the thickness and lateral size of the hexagonal nanoplatelets grow at progressively decreasing rates. The observed slow-down effect in this growth can be assigned to a progressive increase in the weak but not vanishing misfit

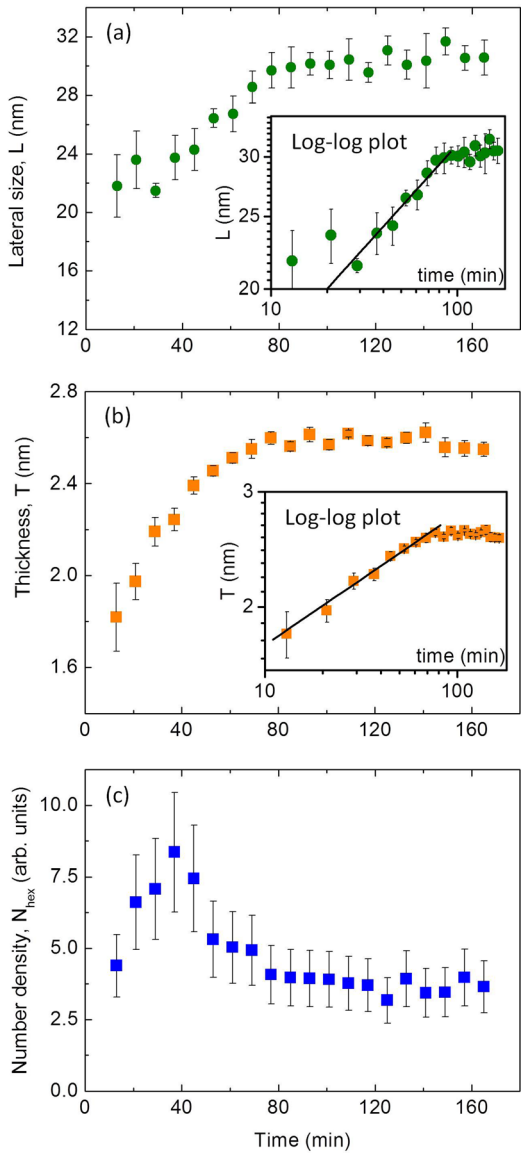

FIG. 3. Time dependences of lateral size (a), thickness (b), and number in relative units (c) of hexagonal $CoSi_2$ nanoplatelets buried in Si(001). The insets in (b) and (c) are the double logarithmic plots of $L(t)$ and $T(t)$, respectively. The slopes in log-log plots before $t = 80$ min indicates that L and T are proportional to $t^{0.27}$ and $t^{0.20}$, respectively.

between the lattice of silicon and that of the coherent $CoSi_2$ nanoplatelets, thus increasing elastic stresses and strains developed in the volume of the silicon host.[9]

The slopes in logarithmic plots in the insets of Figures 3(a) and 3(b) show that the growth of $CoSi_2$ platelets occurs in two different regimes during isothermal treatment at 700 °C. During the first 80 min, the lateral size and thickness of $CoSi_2$ platelets scales as $L \sim t^{0.27}$ and $T \sim t^{0.20}$, respectively (slopes 0.27 and 0.20 in log-log plots). For $t > 80$ min, T becomes time independent and L proportional to $t^{0.04}$. The time exponents corresponding to the first stages of $CoSi_2$ platelets growth are somewhat smaller than the reported for the growth of $CoSi_2$ nanowires in Si,[18,19] where the length and width of the nanowires showed a $t^{1/3}$ time dependence. This difference of time exponents is probably related to differences in deposition conditions. While the growth of nanowires takes place at constant deposition rate of Co,[18,19] in the system investigated here, the concentration of Co atoms in the

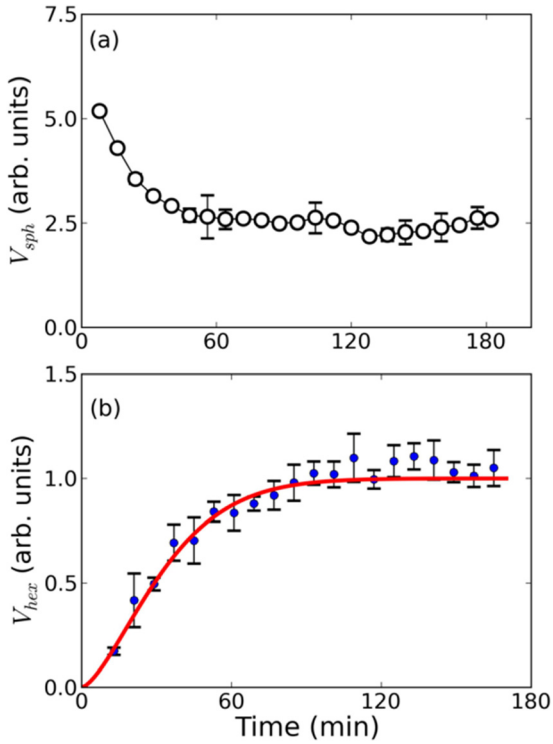

FIG. 4. Time dependences of the total volume of spherical Co nanoparticles (a) and hexagonal $CoSi_2$ nanoplatelets (b). The continuous line in (b) corresponds to the best fit of Avrami equation (Eq. (2)) to the experimental time dependence of nanoplates volume fraction.

SiO_2 thin film decreases, because they feed the growing $CoSi_2$ platelets and Co nanocrystals.

The results plotted in Figure 3(c) indicate that the number of $CoSi_2$ nanoplatelets, N_{hex}, initially increases and then decreases down to its initial value, the magnitude of initial increase being slightly larger than the experimental error bars.

The total volume of Co nanoparticles was derived from the integral of the isotropic part of the scattering intensity,[33] while the total volume corresponding to hexagonal $CoSi_2$ nanoplatelets was calculated from the geometric parameters plotted in Figure 3 as

$$V_{hex}(t) = \frac{3\sqrt{3}}{2} N_{hex} L^2 T. \quad (1)$$

Both calculated volumes, V_{sph} and V_{hex}, are displayed in Figures 4(a) and 4(b), respectively, as functions of the annealing time. It can be noticed in Figure 4(a) that the total volume of Co nanoparticles is a continuously decreasing function down to a final constant value while the total volume of $CoSi_2$ nanoplatelets exhibits an opposite behavior characterized by a continuous increase up to a final value reached after about 80 min of isothermal annealing.

The total volume of Co nanoparticles starts from a maximum value at the beginning of the isothermal process at 700 °C, thus implying that they have nucleated during the prior pre-treatment of the sample at 500 °C. After rising the temperature from 500 °C up to 700 °C, the radii of a fraction of the smaller Co particles (i.e., those belonging to mode I shown in Figure 2), previously formed at 500 °C, become subcritical at 700 °C and, consequently, progressively dissolve during the further isothermal annealing at this temperature.

In order to have a first insight into the mechanism of growth of the $CoSi_2$ nanoplatelets, we have verified if the experimental time dependence of their total volume fraction obeys the theoretical equation proposed by Avrami[34–36]

$$X_V(t) = \frac{V_0 - V_{hex}(t)}{V_0 - V_\infty} = 1 - \exp(-kt^n), \qquad (2)$$

where V_o and V_∞ are the initial and final volumes, respectively, along the transformation process, k is related to the speed of the reaction, and n is a dimension associated to the diffusion process and to the nucleation and growth mechanism.[37]

As can be seen in Figure 4(b), the theoretical time dependence of the volume fraction of nanoplatelets proposed by Avrami (Eq. (2)) fits well to the experimental curve. According to Avrami model, if nucleation is negligible during growth, exponent values are $n = 1$ and $n = 2$ for an invariant number of nanocrystals growing in *one* and *two-dimension*, respectively. The experimental results derived from our GISAXS measurements indicate that the number of $CoSi_2$ platelets remains approximately constant during their growth and the exponent n is 1.5. This suggests that the growth of $CoSi_2$ platelets here investigated proceeds by combined and independent processes governed by *one* and *two-dimension* atomic diffusion, these processes being associated to the observed increase in thickness and in lateral surface area of $CoSi_2$ platelets, respectively.

However, the experimental results plotted in Figure 3(c) indicate a slight increase of N_{hex} followed by a decrease down to its initial value. The complex time dependence of N_{hex} shown in Figure 3(c) is probably a consequence of the simplicity of the model proposed,[9] which assumes a monodisperse set of nanoplatelets along the whole process. This approximation is expected to be good during final stages of growth, when the nanoplatelets have reached their final maximum constant size, but probably is not acceptable during the first stages. On the other hand, the negligible (or absent) nucleation during the growth of platelets, pointed out by the analysis using Avrami model, suggests that the nucleation of nanoplatelets possibly occurs in defects of the external flat Si surface whose number is constant along the whole thermal treatment.

Summarizing, our kinetic study demonstrates that after the prior formation of spherical Co nanoparticles at 500 °C, their number and total volume decreases during isothermal annealing at 700 °C while, contrarily, the total volume of hexagonal $CoSi_2$ nanoplatelets exhibits a parallel increase. Both total volumes of nanoparticles and nanoplatelets reach final values after 80 min of isothermal treatment at 700 °C without any subsequent change.

The opposite trends of the time dependences of the total volume of Co nanoparticles embedded in the SiO_2 thin film and total volume of $CoSi_2$ nanoplatelets buried in Si(001) are the expected consequences of a complex coarsening mechanism that minimizes the total interface area and involves correlated effects of dissolution of Co nanoparticles and parallel growth of $CoSi_2$ nanoplatelets.

We have also shown that the time dependence of the fraction of volume of $CoSi_2$ nanoplatelets is well described by Avrami equation, with its characteristic parameters compatible with the presence of a constant number of supercritical $CoSi_2$ nuclei and independent diffusion processes in one and two dimensions associated to the observed variations in thickness and lateral sizes, respectively.

This work was supported by FAPESP and CNPq (Brazil), CONICET (201101-01035) (Argentina) and National Synchrotron Light Laboratory (LNLS), Campinas, Brazil, through the Project Nos. XRD1-15215 and XPD-17193.

[1]B. M. Boyerinas, A. L. Roytburd, and H. A. Bruck, Nano Lett. **14**, 1818–1822 (2014).
[2]J. M. Higgins, P. Carmichael, A. L. Schmitt, S. Lee, J. P. Degrave, and S. Jin, ACS Nano **5**, 3268–3277 (2011).
[3]S.-Y. Chen, P.-H. Yeh, W.-W. Wu, U.-S. Chen, Y.-L. Chueh, Y.-C. Yang, S. Gwo, and L.-J. Chen, ACS Nano **5**, 9202–9207 (2011).
[4]H. Wang, Z. Zhang, L. M. Wong, S. Wang, Z. Wei, G. P. Li, G. Xing, D. Guo, D. Wang, and T. Wu, ACS Nano **4**, 2901–2909 (2010).
[5]Y.-C. Chou, W.-W. Wu, L.-J. Chen, and K.-N. Tu, Nano Lett. **9**, 2337–2342 (2009).
[6]Y. Lei, W. Cai, and G. Wilde, Prog. Mater. Sci. **52**, 465–539 (2007).
[7]C. L. Hsin, J. H. He, C. Y. Lee, W. W. Wu, P. H. Yeh, L. J. Chen, and Z. L. Wang, Nano Lett. **7**, 1799–1803 (2007).
[8]A. L. Schmitt, M. J. Bierman, D. Schmeisser, F. J. Himpsel, and S. Jin, Nano Lett. **6**, 1617–1621 (2006).
[9]G. Kellermann, L. A. Montoro, L. J. Giovanetti, P. C. dos, S. Claro, L. Zhang, A. J. Ramirez, F. G. Requejo, and A. F. Craievich, Appl. Phys. Lett. **100**, 063116 (2012).
[10]G. Kellermann, L. A. Montoro, L. Giovanetti, P. C. dos, S. Claro, L. Shang, A. Ramirez, F. G. Requejo, and A. Craievich, Phys. Chem. Chem. Phys. **17**, 4945–4951 (2014).
[11]F. Léonard and A. A. Talin, Nat. Nanotechnol. **6**, 773–783 (2011).
[12]C. Chuang, W. Y. Chang, W. H. Chen, J. S. Tsay, W. B. Su, H. W. Chang, and Y. D. Yao, Thin Solid Films **519**, 8371–8374 (2011).
[13]H. A. Atwater and A. Polman, Nat. Mater. **9**, 205–213 (2010).
[14]C.-Y. Lee, M.-P. Lu, K.-F. Liao, W.-W. Wu, and L.-J. Chen, Appl. Phys. Lett. **93**, 113109 (2008).
[15]M. D. Kelzenberg, D. B. Turner-Evans, B. M. Kayes, M. A. Filler, M. C. Putnam, N. S. Lewis, and H. A. Atwater, Nano Lett. **8**, 710–714 (2008).
[16]W. Lu and C. M. Lieber, Nat. Mater. **6**, 841–850 (2007).
[17]K. Kawamura, S. Inagaki, T. Saiki, R. Nakamura, Y. Kataoka, and M. Kase, Jpn. J. Appl. Phys., Part 1 **46**, 7268 (2007).
[18]Z. He, D. Smith, and P. Bennett, Phys. Rev. Lett. **93**, 256102 (2004).
[19]P. A. Bennett, D. J. Smith, Z. He, M. C. Reuter, A. W. Ellis, and F. M. Ross, Nanotechnology **22**, 305606 (2011).
[20]P. A. Bennett, Z. He, D. J. Smith, and F. M. Ross, Thin Solid Films **519**, 8434–8440 (2011).
[21]F. Corni, R. Tonini, G. Ottaviani, S. Alberici, D. Erbetta, and T. Marangon, Microelectron. Eng. **76**, 343–348 (2004).
[22]J. L. Tedesco, J. E. Rowe, and R. J. Nemanich, J. Appl. Phys. **105**, 083721–083727 (2009).
[23]R. C. Chau, B. Doyle, S. Datta, K. Jack, and K. Zhang, Nat. Mater. **6**, 810–812 (2007).
[24]M. Rauscher, T. Salditt, and H. Spohn, Phys. Rev. B **52**, 16855–16863 (1995).
[25]P. Müller-Buschbaum, Anal. Bioanal. Chem. **376**, 3–10 (2003).
[26]G. Renaud, R. Lazzari, and F. Leroy, Surf. Sci. Rep. **64**, 255–380 (2009).
[27]M. Schwartzkopf, G. Santoro, Ca. J. Brett, A. Rothkirch, O. Polonskyi, A. Hinz, E. Metwalli, Y. Yao, T. Strunskus, F. Faupel, P. Müller-Buschbaum, and S. V. Roth, ACS Appl. Mater. Interfaces **7**, 13547–13556 (2015).
[28]S. V. Roth, G. Santoro, J. F. H. Risch, S. Yu, M. Schwartzkopf, T. Boese, R. Döhrmann, P. Zhang, B. Besner, P. Bremer, D. Rukser, M. A. Rübhausen, N. J. Terrill, P. A. Staniec, Y. Yao, E. Metwalli, and P. Müller-Buschbaum, ACS Appl. Mater. Interfaces **7**, 12470–12477 (2015).
[29]M. Schwartzkopf, A. Buffeta, V. Körstgens, E. Metwalli, K. Schlage, G. Benecke, J. Perlich, M. Rawolle, A. Rothkirch, B. Heidmann, G. Herzog, P. Müller-Buschbaum, R. Röhlsberger, R. Gehrke, N. Stribeckb, and S. V. Roth, Nanoscale **5**, 5053 (2013).
[30]C. Revenant, G. Renaud, R. Lazzari, and J. Jupille, Phys. Rev. B **79**, 235424 (2009).

[31]Y.-C. Chou, K.-C. Lu, and K. N. Tu, Mater. Sci. Eng., R **70**, 112–125 (2010).
[32]See supplementary material at http://dx.doi.org/10.1063/1.4936377 for additional description of the GISAXS procedures, analysis, and modeling.
[33]A. Guinier, *Small-Angle Scattering of X-rays* (John Wiley, New York, 1955).
[34]M. Avrami, J. Chem. Phys. **7**, 1103–1112 (1939).
[35]M. Avrami, J. Chem. Phys. **8**, 212–224 (1940).
[36]M. Avrami, J. Chem. Phys. **9**, 177–184 (1941).
[37]T. J. W. De Bruijn, W. A. De Jong, and P. J. Van Den Berg, Thermochim. Acta **45**, 305–314 (1981).